The Journal of Experimental Biology 213, 1651-1658

doi:10.1242/jeb.038109

# Wing and body kinematics of takeoff and landing flight in the pigeon (*Columba livia*)

Angela M. Berg* and Andrew A. Biewener

Harvard University, Concord Field Station, Department of Organismic and Evolutionary Biology, 100 Old Causeway Road, Bedford, MA 01730, USA

*Author for correspondence (amberg@fas.harvard.edu)

Accepted 27 January 2010

## SUMMARY

**Takeoff and landing are critical phases in a flight. To better understand the functional importance of the kinematic adjustments birds use to execute these flight modes, we studied the wing and body movements of pigeons (*Columba livia*) during short-distance free-flights between two perches. The greatest accelerations were observed during the second wingbeat of takeoff. The wings were responsible for the majority of acceleration during takeoff and landing, with the legs contributing only one-quarter of the acceleration. Parameters relating to aerodynamic power output such as downstroke amplitude, wingbeat frequency and downstroke velocity were all greatest during takeoff flight and decreased with each successive takeoff wingbeat. This pattern indicates that downstroke velocity must be greater for accelerating flight to increase the amount of air accelerated by the wings. Pigeons used multiple mechanisms to adjust thrust and drag to accelerate during takeoff and decelerate during landing. Body angle, tail angle and wing plane angles all shifted from more horizontal orientations during takeoff to near-vertical orientations during landing, thereby reducing drag during takeoff and increasing drag during landing. The stroke plane was tilted steeply downward throughout takeoff (increasing from –60±5 deg. to –47±1 deg.), supporting our hypothesis that a downward-tilted stroke plane pushes more air rearward to accelerate the bird forward. Similarly, the stroke plane tilted upward during landing (increasing from –1±2 deg. to 17±7 deg.), implying that an upward-tilted stroke plane pushes more air forward to slow the bird down. Rotations of the stroke plane, wing planes and tail were all strongly correlated with rotation of the body angle, suggesting that pigeons are able to redirect aerodynamic force and shift between flight modes through modulation of body angle alone.**

Supplementary material available online at http://jeb.biologists.org/cgi/content/full/213/10/1651/DC1

Key words: acceleration, bird, perch.

## INTRODUCTION

For most bird species, flying is an essential part of each individual's daily life. Birds fly to forage, to evade predators, to migrate and for numerous other reasons. To be successful, birds not only need to be able to stay aloft but they must also be able to take off from a stationary position and land without injury at the end of the flight. The apparent ease with which most birds accomplish these tasks has, however, resulted in comparatively little study relative to the considerable attention that has been devoted to understanding fundamental aspects of steady forward flight. A successful takeoff typically involves leaping into the air and accelerating to the desired flight speed. When landing, a bird must not slow down too much too early, or it will fall from the air prematurely. Yet, a bird must decelerate enough to be able to gauge the mechanical properties of a perch and to absorb the body's remaining kinetic energy with its legs when it encounters the perch.

Kinematic analysis of takeoff and landing flight modes in previous work has largely been limited to wingbeat frequency and amplitude (Dial, 1992), and general descriptions of the wing-stroke (Brown, 1948; Simpson, 1983), or has focused on only one flight mode, hindering comparison among flight modes (Green and Cheng, 1998; Earls, 2000; Tobalske and Dial, 2000; Tobalske et al., 2004). In the rock pigeon (*Columba livia*, Gmelin 1798), wingbeat frequency has been found to be similar during level flight and landing, but greater during takeoff (Dial, 1992). In the same study, wingbeat amplitude was higher during takeoff and landing, compared with level flight. The present study explores more broadly and in more detail the kinematic parameters of both takeoff and landing, with the goal of identifying the wing and body kinematics that produce accelerating and decelerating flight.

Most previous work on takeoff and landing has focused on muscle function and power requirements (e.g. Dial, 1992; Biewener et al., 1998; Tobalske and Dial, 2000; Askew et al., 2001; Usherwood et al., 2005). Several of these studies have compared takeoff and landing in order to explore the range of flight muscle function. In pigeons, several wing muscles show the strongest activation during takeoff from the ground or landing on a perch (Dial, 1992). However, compared with mid-flight, the large, anterior sternobrachial region of the pectoralis (the main downstroke muscle) performs less work during takeoff from a perch and more work during the initial phases of landing flight (Biewener et al., 1998). The supracoracoideus (the main upstroke muscle) also generates lower stress and fascicle strain, and thus less power, during takeoff and landing when compared with mid-flight (Tobalske and Biewener, 2008). Finally, consistent with theory, differential pressure measurements suggest greater aerodynamic power production at distal regions of the wing during takeoff and landing, when birds are flying slowly and accelerating or decelerating (Usherwood et al., 2005).

Intrinsically, takeoff and landing involve changes in flight speed. Previous studies have more often examined the kinematics and power requirements when birds fly steadily over a range of speeds in a wind tunnel (Tobalske and Dial, 1996; Tobalske et al., 2003; Hedrick et al., 2004; Rosen et al., 2004). These studies have shown that in several bird species, wingbeat frequency varies little across flight speeds. However, body angle decreases with increasing speed

in several species (Tobalske and Dial, 1996; Tobalske et al., 2003; Hedrick et al., 2004). Tobalske and colleagues found that stroke plane angle becomes more vertical and wing excursion increases with increasing flight speeds in budgerigars (*Melopsittacus undulates*), cockatiels (*Nymphicus hollandicus*), ring-neck doves (*Streptopelia risoria*) and black-billed magpies (*Pica hudsonia*) (Tobalske et al., 2003). In contrast, Rosen and colleagues found that the inclination angle of the wingtip path in a thrush nightingale (*Luscinia luscinia*) becomes steeper with decreasing flight speeds, and that wingbeat amplitude does not depend on flight speed (Rosen et al., 2004). These differing results indicate that species can differ in these kinematic flight parameters. Familiarity with a perch can also affect the speed at which a bird will land. Green and Cheng found that pigeons approach more quickly as they become familiar with a perch (Green and Cheng, 1998).

This paper presents the first of a series of investigations we have undertaken to analyze the mechanisms of takeoff and landing flight in birds. The aim of this study was to understand the underlying kinematics of takeoff and landing maneuvers in a generalist flyer. Pigeons were conditioned to fly between two perches while their movements were recorded with high-speed video. Because takeoff and landing require accelerations in opposite directions, we expected to observe vastly different kinematics between these two flight modes. To accelerate forward during takeoff, we expected birds to exhibit greater wing stroke amplitudes in order to accelerate more air. We also expected the tail to be narrower during takeoff in order to reduce drag. We assumed that the wings could be modeled with a simple actuator disk model where air is accelerated in the direction normal to the stroke plane. Based on this assumption, we expected the stroke plane angle to be tilted steeply downward during takeoff to accelerate more air rearward and the bird forward. In contrast, during landing flight, we expected the stroke plane angle to be tilted upward to accelerate more air forward, thereby slowing the bird down. Compared with takeoff and mid-flight, we expected faster wing velocity during landing flight in order to increase drag on the wing and assist in decelerating the bird.

## MATERIALS AND METHODS

### Animals and flight arena

Rock pigeons were housed at the Concord Field Station in Bedford, MA, USA, and provided with food and water *ad libitum*. All experiments were conducted in accordance with institutional animal care and use guidelines. Birds were trained regularly to fly between two perches 6–8 m apart. The training period included dozens of successful takeoffs and landings, which prevented the potentially confounding effects of a pigeon encountering a novel perch (Green and Cheng, 1998). The perches were made of wood dowels 2.5 cm in diameter, covered with tape to provide a gripping surface for the birds, and mounted on wooden stands 1 m tall.

### Kinematic data collection

Data from seven birds (431±67 g, mean body mass ± standard deviation) were used to obtain detailed kinematics. Three to four high-speed digital cameras were positioned around the flight corridor. Depending on circumstances, one Photron FastCam-X 1280 PCI camera, one or two Photron FastCam 1024 PCI cameras (Photron USA Inc., San Diego, CA, USA), and zero to two RedLake PCI 500 cameras (RedLake Inc., San Diego, CA, USA) were used. Cameras recorded at 250 frames $s^{-1}$ with shutter speeds of 1/500 to 1/2000 s. Cameras were calibrated using the direct linear transform method (Hatze, 1988) and the MatLab$^{TM}$ (version 7.4; 2007, The MathWorks, Inc., Natick, MA, USA) script *DLTcalibration.m* written by Ty Hedrick (Hedrick, 2008). All axes were defined in the global reference frame. The *x*-axis was defined as the axis along the flight corridor; the *y*-axis as perpendicular to the *x*-axis and in the horizontal plane; and the *z*-axis as the vertical.

Prior to data collection, all birds were marked with non-toxic, high-contrast ink at several anatomical landmarks: wing root (as a proxy for the shoulder), wrist, wingtip (9th primary feather), rump, and three points on the trailing edge of the tail (Fig. 1A). Birds 1–5 were also marked on the 6th primary feather and 2nd secondary feather. The straightest, most level flights for each bird were selected for analysis. After data collection, the marked points on the wing nearest the camera were digitized using the MatLab$^{TM}$ script *DLTdv3.m* written by Ty Hedrick (Hedrick, 2008). Position data were filtered with a low-pass Butterworth filter at four times the average wingbeat frequency for the filmed portion of the flight. Three takeoff flights and three landing flights were analyzed for birds 1–5. For this study, four mid-flights were analyzed for birds 2, 4, 6 and 7.

### Kinematic calculations

Wingbeat phase was determined by the position of the wingtip in the *y*-axis, relative to the wing root. Mediolateral (*y*-axis) endpoints of the wingtip path were used to identify the points of wing reversal: the upstroke–downstroke transition (USDS) and the downstroke–upstroke transition (DSUS) were designated as the times when the wingtip was most medial to the wing root, and dorsal or ventral to the bird's body, respectively. One wingbeat was designated as the time from one USDS to the next USDS. Mid-downstroke was designated as the time when the wingtip was farthest from the wing root in the *y*-direction during the downstroke.

Because the birds did not always touch down onto the perch at the same wingbeat phase, it was necessary to standardize the wingbeat numbers relative to the moment the feet touched the perch ('footdown'). The zeroth wingbeat was defined as the wingbeat that ended either after footdown, or less than 20 ms before footdown. In other words, the USDS that occurred after footdown or less than 20 ms before footdown defined the end of 'wingbeat 0'. The wingbeats were then counted backwards in time as wingbeats –1, –2 and –3. During takeoff, birds consistently left the perch after the first USDS and before the first mid-downstroke. This first USDS defined the beginning of wingbeat 1, which was followed by wingbeats 2, 3 and 4. For each flight, four wingbeats (five USDSs) were analyzed, with the exception of two takeoffs and one landing for bird 2 where only three wingbeats were recorded (wingbeats 1 to 3 of takeoff and –2 to 0 of landing).

The mid-back of the bird was approximated by using the *y*-coordinate of the rump and the average of the *x*-coordinates of the rump and wing root. This point served as a proxy for the center of mass, which was not measured on these birds. Whole-body horizontal velocity ($\mathbf{V}_x$) was calculated by differentiating mid-back position data along the *x*-axis. To reduce the effects of inertia on acceleration estimates, instead of differentiating velocity, we used the following method to calculate the average horizontal acceleration of the body over the wingbeat ($\mathbf{A}_{x,\mathrm{wb}}$). $\mathbf{V}_x$ values were averaged from one time step before USDS to one time step after USDS to obtain a mean $\mathbf{V}_x$ at USDS. The difference between the mean $\mathbf{V}_x$ values at sequential USDSs gave $\mathbf{A}_{x,\mathrm{wb}}$.

The wing markers on birds 1–5 allowed three distinct wing planes to be analyzed: the arm wing, the proximal hand wing and the distal hand wing, as illustrated in Fig. 1A. The vertical angle of these wing planes was determined as the angle between the plane and the horizontal (Fig. 1A,B). Tail angle was also calculated as the angle between the tail plane and the horizontal (Fig. 1B). The tail plane

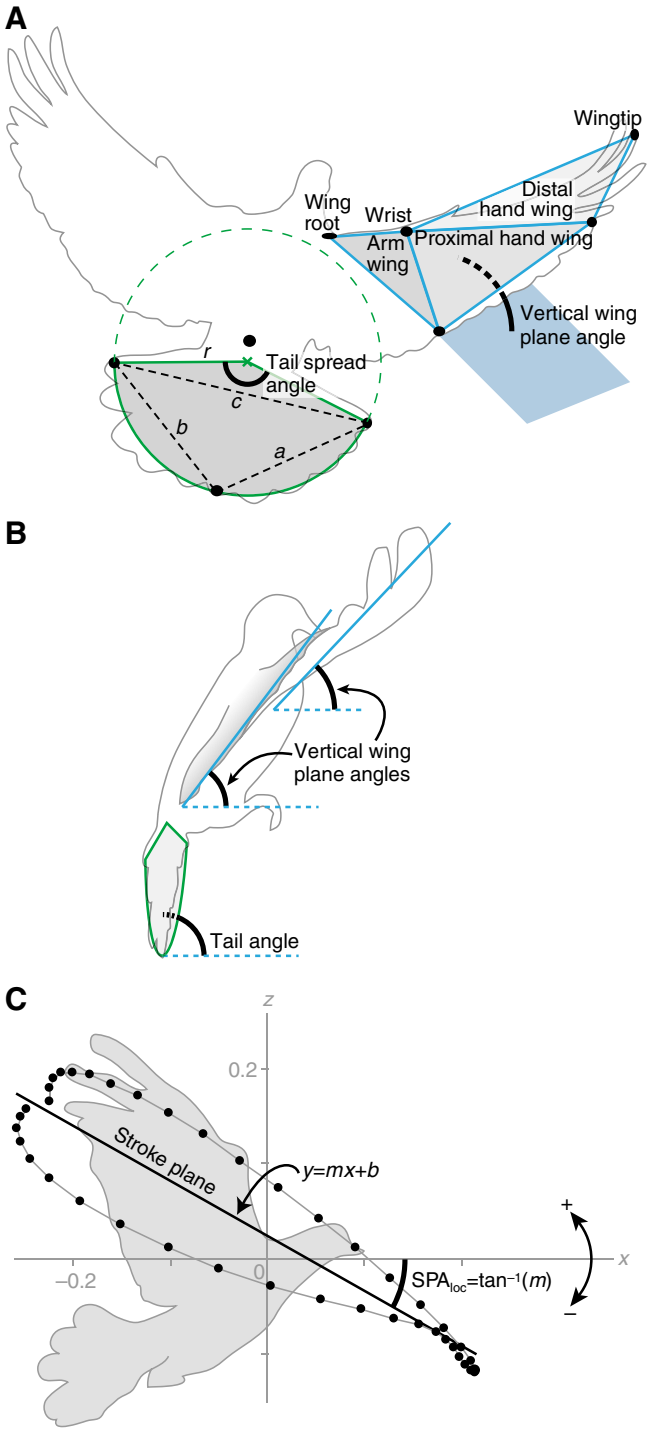


Fig. 1. Calculation of the wing and tail angles (A,B) and the local stroke plane angle (SPA$_{loc}$; C). Triangles defining the wing and tail planes were based on the digitized points (A). Tail spread was calculated using the assumption that the tail formed a wedge of a circle, as described in the text. The vertical wing and tail angles were calculated as the angle between the plane and the horizontal (A,B). The blue plane in A and the blue dashed lines in B represent the horizontal. For each wingbeat, the linear regression of the *x*- and *z*-coordinates of the wingtip position relative to the shoulder was calculated (C). SPA$_{loc}$ is the angle corresponding to the slope of the linear regression. SPA$_{loc}$ is negative when the wingtip moves forward and downward during downstroke (as illustrated here), and positive when the wing moves forward and upward during downstroke (as in landing). The global downstroke plane angle (DSPA$_{glob}$) was calculated in a similar manner, using wingtip position in the global coordinate system instead.

was defined by the three marks on the trailing edge of the tail. Because of the mobility of the tail relative to the rump mark, the rump was not used to determine tail spread. Instead, the trailing edge marks were used to determine the tail spread using the following method. Because the trailing edge of the tail feathers forms a nearly circular arc when spread, the tail was assumed to be a portion of a circle (Fig. 1A). The radius, *r*, of this circle was determined using the equation:

$$r = \frac{abc}{\sqrt{2a^2b^2 + 2b^2c^2 + 2c^2a^2 - a^4 - b^4 - c^4}}, \quad (1)$$

where *a*, *b* and *c* are each a distance between two of the trailing edge marks (Fig. 1A). The tail spread was then calculated as:

$$\text{Spread} = 2\sin^{-1}\frac{a}{2r} + 2\sin^{-1}\frac{b}{2r}, \quad (2)$$

using two terms with *a* and *b* (instead of one term with *c*) in order to permit values greater than 180 deg.

Stroke plane angles (SPAs) were calculated using the wingtip path projected onto the *x*–*z* plane. Because the SPAs changed sign during the flights, SPAs were calculated as the arctangent of the slope of the linear regression of the projected path, with the sign as indicated in Fig. 1C (a downward-tilted stroke plane corresponding to a negative SPA, and an upward-tilted stroke plane corresponding to a positive SPA). The local SPA (SPA$_{loc}$) used the wingtip path relative to the wing root for the entire wingbeat. The global downstroke plane angle (DSPA$_{glob}$) used the wingtip path in the global coordinate system of the downstroke only. Body angle was calculated as the angle between the horizontal and the line connecting the wing root and the rump, also projected onto the *x*–*z* plane. Protraction was calculated as the distance from the SPA$_{loc}$ to the wing root in the *x*–*z* plane.

Downstroke sweep angle (θ) is a measure of stroke amplitude that accounts for angular motion of the stroke. The angle through which the wingtip swept at each time step was summed over the entire downstroke to give θ. The value of θ was divided by the duration of the downstroke to give the downstroke sweep velocity (ω).

Kinematic analyses were performed using custom-written MatLab™ scripts.

### Statistical analysis

For each flight, the wingbeats were numbered as described above. For each bird, parameter values for wingbeats of the same number were averaged among the flights for that bird. This procedure gave series of mean values to describe the numbered wingbeats of each bird. Mean values for wingbeats of the same number were averaged among all birds, giving the grand mean for each parameter for each wingbeat number. Unless otherwise noted, values reported are grand means. Repeated-measures analyses by both bird and wingbeat were performed in SPSS (version 16.0; SPSS Inc., Chicago, IL, USA). Linear regressions and *t*-tests were performed in Microsoft Excel (2007; Microsoft Corp., Redmond, WA, USA). To account for multiple comparisons, the sequential Bonferroni method (Rice, 1989) was used to test for significance of differences observed in sets of repeated-measures analyses and in sets of *post hoc* *t*-tests. Values are reported as means ± standard deviation.

## RESULTS

### Whole-body kinematics

#### Velocity and acceleration

Along the portions of the flight path analyzed for takeoff, most birds continuously increased their horizontal velocity (Fig. 2A;

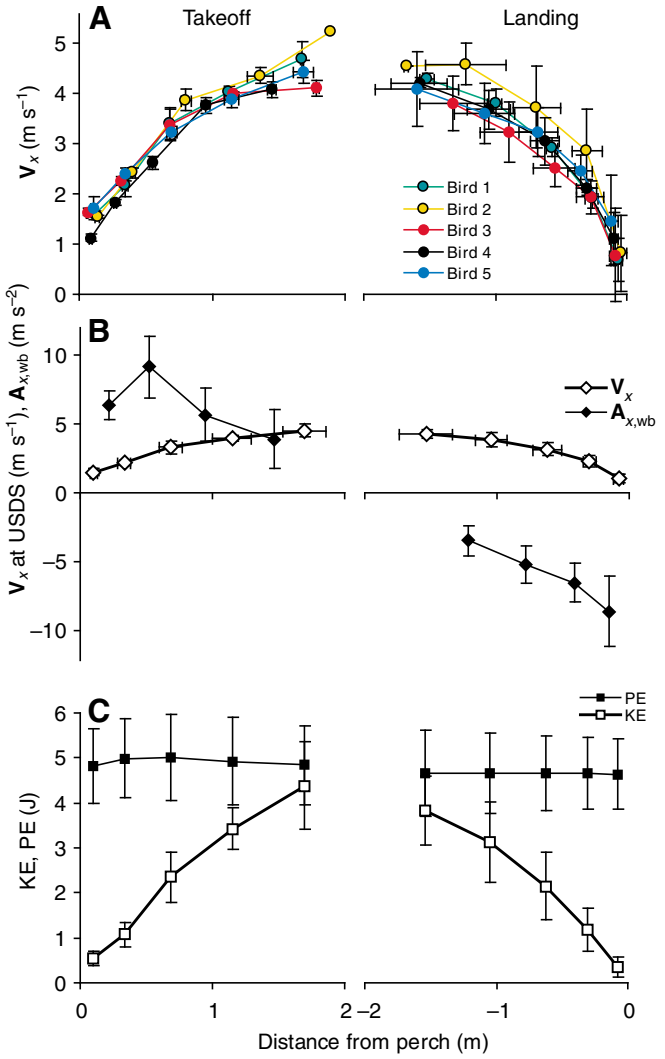


Fig. 2. Whole-body kinematics: individual means of bird velocity in the *x*-direction ($\mathbf{V}_x$) at the upstroke–downstroke transitions (USDSs; A); grand means of $\mathbf{V}_x$ at USDSs and acceleration in the *x*-direction over the course of the wingbeat ($\mathbf{A}_{x,wb}$; B); and kinetic and potential energies (KE and PE; C). Points for $\mathbf{V}_x$, KE and PE indicate data for each USDS. Points for $\mathbf{A}_{x,wb}$ indicate data for each wingbeat. Horizontal error bars on $\mathbf{V}_x$ indicate the standard error in the distance from the perch at each USDS. Colors represent individual birds. For each point in A, $N$=3, with the exception of the 5th and 6th points for bird 2, for which $N$=1 and $N$=2, respectively (further detail is provided in the text). $\mathbf{V}_x$ increased for all individuals after leaving the perch during takeoff (A). During landing, $\mathbf{V}_x$ decreased for all individuals prior to encountering the perch but was more variable than during takeoff. $\mathbf{A}_{x,wb}$ was greatest during the second wingbeat of takeoff, and became increasingly negative during landing. As expected, KE followed the pattern observed for $\mathbf{V}_x$, and PE did not change during takeoff or landing (C). Thus, in the flights analyzed, there was no tradeoff between KE and PE.

supplementary material Movie 1). Likewise, in the portion of landing analyzed, most birds continuously decreased their velocity (supplementary material Movie 2). Whole-body velocity varied within individuals more during landing than during takeoff. During takeoff, the horizontal velocity ($\mathbf{V}_x$) was 1.52±0.23 m s$^{-1}$ at the beginning of wingbeat 1, when the feet were leaving the perch; and 4.51±0.48 m s$^{-1}$ at the end of wingbeat 4 (Fig. 2B). During landing, $\mathbf{V}_x$ was 4.19±0.27 m s$^{-1}$ at the beginning of wingbeat –3, and 0.97±0.32 m s$^{-1}$ at the end of wingbeat 0.

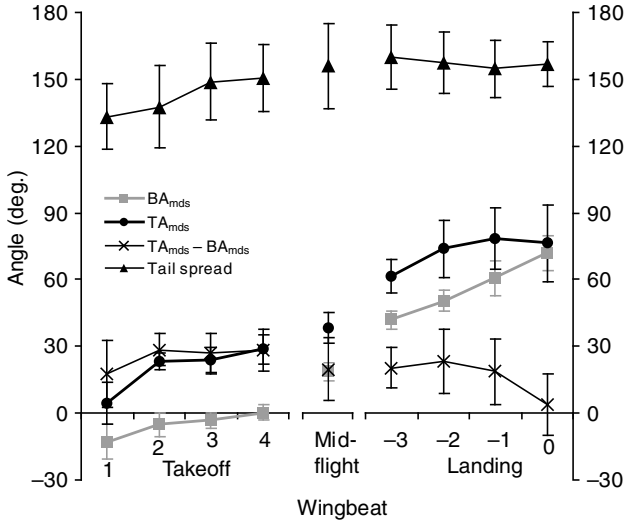


Fig. 3. Body and tail angles at mid-downstroke for each wingbeat. Body angle and vertical tail angle ($BA_{mds}$ and $TA_{mds}$, respectively) both increase continually throughout takeoff and landing, with total increases of 85 deg. and 74 deg., respectively. Consequently, $TA_{mds}$ relative to $BA_{mds}$ ($TA_{mds} - BA_{mds}$) does not differ significantly among wingbeats (*t*-tests, $P \geq 0.004$ for all comparisons, non-significant by sequential Bonferroni). Tail spread increased somewhat from takeoff to landing, but did not vary significantly among wingbeats (repeated-measures, $F$=1.745, $P$=0.125).

Acceleration in the *x*-direction over the course of the wingbeat ($\mathbf{A}_{x,wb}$) was greatest for wingbeat 2 (9.14±2.22 m s$^{-2}$) during takeoff and decreased during subsequent wingbeats (Fig. 2B). During landing, $\mathbf{A}_{x,wb}$ became more negative, with wingbeat 0 exhibiting the most negative $\mathbf{A}_{x,wb}$ (–8.50±2.52 m s$^{-2}$). As expected, kinetic energy (KE) followed $\mathbf{V}_x$, increasing during takeoff and decreasing during landing (Fig. 2C). Because the most level flights between the perches were selected for analysis, potential energy (PE) did not change significantly during the takeoffs or landings (repeated-measures, $F$=1.778, $P$=0.117; Fig. 2C). Generally, the pigeons did not land from distances sufficiently above or below the perch to alter their PE under the experimental flight conditions.

### Body and tail angles

Body angle fluctuated during each wingbeat, reaching its steepest angle at or just after the USDS (supplementary material Movies 1–3). During takeoff, the body angle was shallowest near the end of downstroke. During landing and mid-flight, the body angle was shallowest near mid-downstroke. Body angle at mid-downstroke ($BA_{mds}$) increased dramatically over the course of the flight (Fig. 3). $BA_{mds}$ averaged –13.0±7.9 deg. for wingbeat 1, indicating that the wing root was below the rump for the first wingbeat. During mid-flight, $BA_{mds}$ was 19.0±9.3 deg., and by wingbeat 0, $BA_{mds}$ was 72.0±7.8 deg. Birds occasionally pitched beyond the vertical during the final landing wingbeat, resulting in a body angle that exceeded 90 deg.

Tail angle also fluctuated during each wingbeat. Although the timing patterns of maximum and minimum tail angle varied among individuals, for landing it was frequently observed that the tail was at its steepest at the DSUS and at its shallowest during mid-downstroke. Like body angle, tail angle at mid-downstroke ($TA_{mds}$) generally increased over the course of the flight (Fig. 3), averaging 4.4±9.3 deg. for wingbeat 1 and increasing to 78.3±13.7 deg. for wingbeat –1. Both $TA_{mds}$ and $BA_{mds}$ increased over 70 deg. from takeoff to landing. As a result, $TA_{mds}$ relative to $BA_{mds}$ did not vary

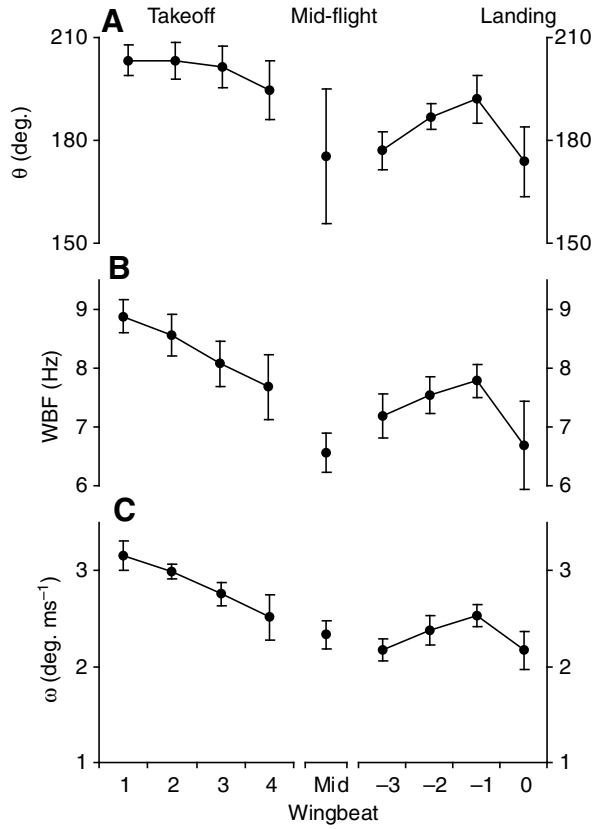


Fig. 4. Downstroke sweep angle (θ; A), wingbeat frequency (WBF; B) and downstroke sweep velocity (ω; C) for each wingbeat. θ, a measure of wingbeat amplitude, is greatest during takeoff (A). θ remains consistent during takeoff, but increases during landing before dropping at the final wingbeat. WBF declines during takeoff, but also increases during landing before dropping at the final wingbeat (B). ω thus follows a similar pattern to both θ and WBF (C).

significantly among wingbeats (repeated-measures, $F$=1.743, $P$=0.125). The tail was broadly spread throughout the flights, averaging 151±18 deg. over all wingbeats. Although mean tail spread at mid-downstroke increased somewhat from takeoff to landing, it did not vary significantly among wingbeats (repeated-measures, $F$=1.745, $P$=0.125).

## Wing kinematics

### Wing velocity

Similar patterns of downstroke sweep angle (θ), wingbeat frequency (WBF) and, thus, downstroke sweep velocity (ω), were observed across the three phases of flight examined (Fig. 4). θ usually remained above 180 deg. throughout the flights (Fig. 4A). Values of θ above 180 deg. were reached for multiple reasons: the wingtip traveled medial to the wing root, the wingtips often crossed at USDS and DSUS, and sweep angle as calculated here (in contrast to simple stroke amplitude) accounts for curvature in the wing stroke path. Values of θ differed significantly among wingbeats (repeated-measures, $F$=8.669, $P$<0.001) and were greatest during the first two wingbeats of takeoff (203±5 deg.). During landing, θ increased from the mid-flight value of 176±17 deg. until reaching a maximum of 192±7 deg. at wingbeat –1, after which it decreased significantly to 174±10 deg. during wingbeat 0 ($t$-test, $P$=0.002). WBF varied significantly among wingbeats (repeated-measures, $F$=15.850, $P$<0.001). WBF declined steadily during takeoff, from 8.88±0.28 $s^{-1}$ at wingbeat 1 to 7.68±0.56 $s^{-1}$ at wingbeat 4 (Fig. 4B). During mid-flight, WBF averaged 6.57±0.30 $s^{-1}$, which was significantly lower than all other wingbeats except wingbeat 0 ($t$-tests, $P$=0.367 *vs* wingbeat 0, $P$<0.001 *vs* all other wingbeats). Similar to the pattern seen for θ, WBF increased during landing, reaching a maximum at wingbeat –1 (7.78±0.25 $s^{-1}$) before decreasing significantly for wingbeat 0 (6.81±0.67 $s^{-1}$; $P$<0.001). Because θ and WBF followed similar patterns, ω also showed a similar pattern (Fig. 4C) and showed significant variation among wingbeats (repeated-measures, $F$=25.064, $P$<0.001). Values of ω declined during takeoff from 3.16±0.16 deg. $ms^{-1}$ for wingbeat 1 to 2.51±0.23 deg. $ms^{-1}$ for wingbeat 4. During landing, ω increased to a maximum at wingbeat –1 (2.45±0.11 deg. $ms^{-1}$) before decreasing significantly for wingbeat 0 (2.11±0.19 deg. $ms^{-1}$; $P$=0.002).

### Wingtip patterns and stroke plane angles

Fig. 5 shows the path of the wingtip during an example takeoff, mid-flight and landing of bird 2. During most wingbeats of takeoff and landing, the birds' wingtips traced a figure-of-eight pattern relative to the shoulder in the lateral view. During mid-flight, the wingtips of most birds traced a path around the shoulder, though some birds' wingtips still showed a figure-of-eight pattern. The compressed appearance of the wingtip path in the dorsal view during takeoff is due to the steep SPA relative to the horizontal plane. The wingtip traces from the lateral view illustrate the shift in the SPAs from negative during takeoff to positive during landing. $SPA_{loc}$ varied significantly among wingbeats (repeated-measures, $F$=219.309, $P$<0.001) and was greater during landing wingbeats than during takeoff wingbeats ($P$<0.001 for all such comparisons; Fig. 6A). During takeoff, $SPA_{loc}$ increased from –60.8±5.3 deg. for wingbeat 1 to –47.5±1.0 deg. for wingbeat 4 (Fig. 6B). During mid-flight, $SPA_{loc}$ averaged –29.5±5.5 deg. During landing, $SPA_{loc}$ increased from –0.9±1.7 deg. during wingbeat –3 to 17.3±7.4 deg. during wingbeat 0. The $SPA_{loc}$ relative to the $BA_{mds}$ ($SPA_{relBA}$) was restricted to a much narrower range during flight, averaging –48.2±7.0 deg. over all three modes of flight (mean of all flights; Fig. 6B). $SPA_{relBA}$ differed significantly among wingbeats (repeated-measures, $F$=5.947, $P$<0.001), but *post hoc* comparisons did not show systematic differences related to flight mode. The $DSPA_{glob}$ showed changes similar to $SPA_{loc}$, increasing steadily from –60.5±5.6 deg. at wingbeat 1 during takeoff to 13.1±7.0 deg. at wingbeat 0 during landing (Fig. 6B).

Wing protraction decreased slightly but not significantly during takeoff ($P$>0.003 for each comparison; Fig. 6C) averaging 8.1±1.7 cm over all takeoffs, but increased during landing from 6.2±2.0 cm during wingbeat –3 to 10.7±1.3 cm for wingbeat 0. Wing protraction was significantly greater for wingbeat 0 than for all other wingbeats ($P$≤0.002 for each comparison), while during mid-flight it was significantly lower than for all other wingbeats (2.7±2.5 cm; $P$<0.001 for each comparison). The vertical angles of the three wing planes (illustrated in Fig. 1A,B) all increased more than 90 deg. from takeoff to landing (Fig. 6B). The plane angles did not differ significantly from each other in most instances ($t$-tests; $P$>0.008 for 18 of 24 comparisons; $P$≤0.002 for arm wing *vs* proximal and distal hand wings in wingbeat 4, arm wing *vs* proximal hand wing in wingbeats –2, –1 and 0, and proximal *vs* distal hand wings in wingbeat –2).

### Correlation of body and wing angles

The angle of several features – stroke planes, wing planes and tail – increased from takeoff to landing, in concert with the increase in $BA_{mds}$ (Fig. 7). The $SPA_{loc}$ was highly correlated with body angle ($R^2$=0.950). Notably, the coefficient of the regression of $SPA_{loc}$

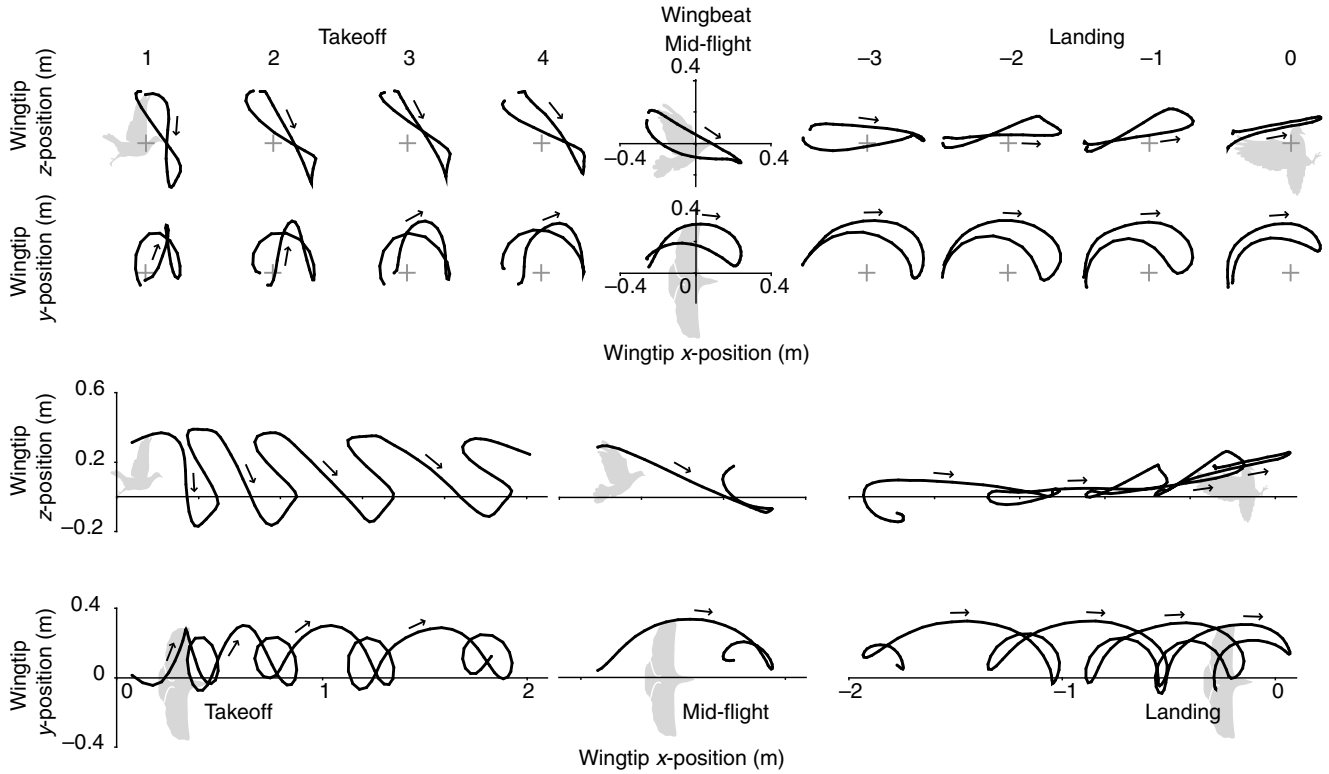


Fig. 5. Example kinematic traces for takeoff, mid-flight and landing for bird 2. Arrows indicate the direction of wingtip movement during downstroke. Top panels show wingtip position relative to the shoulder for each wingbeat. Gray crosses indicate the location of the shoulder when the origin is not shown. Lower panels show wingtip position in the global coordinate system, with tick marks indicating distance from the perch. The traces illustrate the changes in stroke planes from negative angles during takeoff and mid-flight to positive angles during landing. The steeply tilted stroke planes during takeoff account for the compressed appearance of the wingtip path in the dorsal view during takeoff. These trends in stroke plane angle (SPA) are evident for both local and global coordinate systems.

against body angle (0.99) reflects the uniformity of $SPA_{relBA}$ across wingbeats, and the constant (–48.0) reflects the typical value of $SPA_{relBA}$ measured for individual wingbeats (–48.2±7.0 deg.). Increases in wing plane angles were also highly correlated with increases in body angle (arm wing: $R^2$=0.925; proximal hand wing: $R^2$=0.950; distal hand wing: $R^2$=0.957). The changes in tail angle were also correlated with changes in body angle ($R^2$=0.783).

## DISCUSSION

In this study we sought to distinguish important differences in wing and body kinematics among takeoff, mid-flight and landing in the pigeon, with the goal of interpreting these patterns in the context of their possible aerodynamic significance. During takeoff, we found that pigeons continued to accelerate after leaving the perch. Earls found that at the instant that starlings (*Sturnus vulgaris*) and quail (*Coturnix coturnix*) leave the ground during takeoff, they have already achieved 80–90% of the velocity they will reach by the following USDS (Earls, 2000). For hummingbirds taking off from a perch, this value is far less – 59% (Tobalske et al., 2004). When the pigeons here broke contact with the perch, they were in the early moments of the first downstroke, yet they had achieved 74±10% of the velocity reached by the next USDS. Consequently, most of the acceleration into flight is the result of push-off from the legs. However, after the first takeoff wingbeat, the pigeons in this study continued to accelerate during the next three wingbeats. Thus, like starlings and quail, pigeons use their legs to provide most of the acceleration for the first wingbeat, but the wings subsequently provided significant acceleration to achieve the velocities of mid-flight. Bonser and Rayner found that when starlings land, they exert less force on the perch than when taking off, suggesting that starlings decelerate prior to placing their feet on the perch (Bonser and Rayner, 1996). Consistent with this, we found that by the final USDS of landing, pigeons slowed to a quarter of the speed recorded prior to landing, showing that most of the deceleration occurred during flight.

As expected, we found that downstroke amplitude and wingbeat frequency were greatest during takeoff flight, consistent with earlier observations (Dial, 1992). Sweeping the wing through a greater amplitude increases the amount of air that the wing accelerates, increasing the lift and drag it experiences. We hypothesized that a greater wing velocity during landing would result in greater rearward force on the wing because the wings are oriented vertically and the downstroke is directed forward during landing. A greater rearward force on the wings would increase drag (i.e. force directed opposite the direction of travel) and slow the bird. But contrary to our expectation, downstroke sweep velocity was highest during takeoff. This observation likely reflects the need to produce greater upward force during takeoff. In takeoff, the wings are oriented horizontally and the downstroke is directed downward. In this arrangement, we hypothesize that the force produced by the wings is directed more upward, which would help the bird leave the perch and stay aloft at the low speeds of the first wingbeats of takeoff.

As past workers have noted (e.g. Tobalske and Dial, 1996; Usherwood et al., 2005), the tail is broadly spread in pigeons during flight at low speeds, including the takeoff and landing phases. But contrary to our expectations, the tail was not spread significantly more during landing to increase drag, nor significantly less during

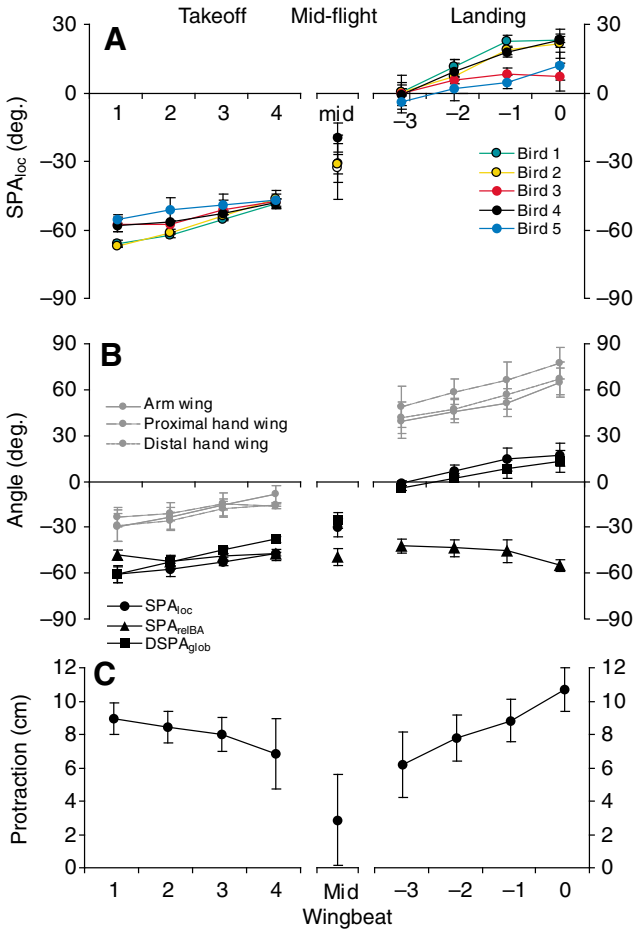


Fig. 6. Wing kinematics: individual means of $SPA_{loc}$ (A), grand means of SPAs and wing plane angles at mid-downstroke (B) and wing protraction (C). (A) For all individuals, $SPA_{loc}$ increased during takeoff and landing, changing sign from negative during takeoff to positive by the end of landing. Colors represent individual birds, with open circles at mid-flight representing birds 6 and 7, for whom only mid-flight data were available. (B) $SPA_{loc}$ increased 78 deg. from the first wingbeat to the last, corresponding with the 85 deg. increase in body angle (Fig. 3). The $SPA_{loc}$ relative to the body angle ($SPA_{relBA}$) thus changes relatively little during these flights. $DSPA_{glob}$ closely followed $SPA_{loc}$. The vertical angles of the wing planes at mid-downstroke all increased during takeoff and landing and were generally not significantly different from each other (see text for explanation of statistics). (C) Protraction of the wing, calculated as the distance between the local stroke plane and the shoulder, did not change significantly during takeoff ($P$>0.003 for each comparison), but increased during landing and by wingbeat 0 was greater than during all other wingbeats ($P$≤0.002 for each comparison).

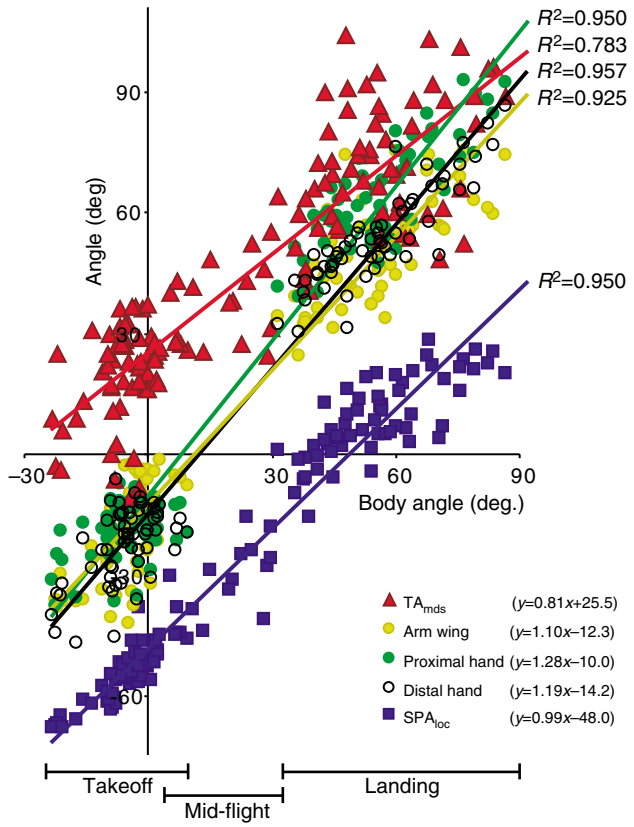


Fig. 7. Scatter plots and least-square linear regressions of stroke plane, wing plane and tail angles plotted against $BA_{mds}$. Labeled brackets indicate body angle ranges for each mode of flight. All of these angles increased similarly from takeoff to landing. Increases in $SPA_{loc}$ and vertical wing plane angles were highly correlated with increases in body angle ($R^2$>0.92 for each). In addition, the coefficient of 0.99 in the regression equation for $SPA_{loc}$ reflects the uniformity of the $SPA_{loc}$ relative to body angle. $TA_{mds}$ was also correlated with body angle ($R^2$=0.783). By controlling the orientation of the body as a whole, pigeons control the stroke plane, wing plane and tail angles, thereby adjusting thrust and drag production and the direction of aerodynamic force.

takeoff to decrease drag. This suggests that pigeons do not use tail spread as a mechanism to modify the magnitude or orientation of aerodynamic force during takeoff and landing.

We found that the wing was most protracted during the end of landing, when flight velocity was lowest and body angle highest. A more protracted wing posture is also observed during the slow descending flights of pigeons (Berg and Biewener, 2008), suggesting that pigeons maintain more protracted wing positions during slower flights with steep body angles. By shifting the plane of force generation produced by the wings farther above the body's center of mass through a more protracted wing stroke, pigeons may increase their stability during such flight behaviors.

Surprisingly, several kinematic parameters rotated through large angles in concert from takeoff to landing (Fig. 7). Both the $SPA_{loc}$ and the $DSPA_{glob}$ increased over 70 deg. from takeoff to landing (Fig. 6B). The downward tilt of the $SPA_{loc}$ during takeoff would have increased the forward thrust (i.e. force in the direction of travel) by pushing more air rearward and thus directing the aerodynamic force more forward. The upward tilt of the $SPA_{loc}$ during landing would have pushed more air forward, directing the aerodynamic force more rearward. We also found that body angle, tail angle and wing plane angles all increased more than 70 deg. from takeoff to landing (Fig. 3). Although we believe the rotation of the stroke plane to be the most important consequence of body rotation, the coordinated changes in body and wing orientation likely reduced the drag (i.e. force directed opposite to the direction of travel) on the bird during takeoff to assist in acceleration, and increased drag during deceleration and landing. The figure-of-eight shape of the wingtip paths in the lateral view during both takeoff and landing was similar to that observed in pigeons during slow ascending, level and descending flight (Tobalske and Dial, 1996; Berg and Biewener, 2008), but the rotation of the figure-of-eight pattern makes apparent the shift in SPA from a steep downward tilt during takeoff to an upward tilt during landing (Fig. 5).

Although the shift in SPA was expected, we did not anticipate the highly correlated increases in body, tail and wing plane angles. It thus appears that pigeons rotate several features – body, wing, tail and stroke plane – to decrease drag and increase thrust during takeoff, and to increase drag and decrease forward thrust during landing; yet, all of these changes are effected by simply rotating the body as a whole (Fig. 7). Pigeons appear to exhibit stereotypic SPAs across flight modes, similar to the findings of Dial and colleagues (Dial et al., 2008), except that the chukars in their work showed consistent SPAs in the gravitational reference frame (Dial et al., 2008), whereas the pigeons in the present study showed consistent SPAs relative to the body [$SPA_{relBA}$ here, the 'vertebral' reference frame of Dial et al. (Dial et al., 2008)]. Importantly, this finding suggests two alternative hypotheses regarding flight muscle activation and contractile patterns. The subtle changes in wing kinematics relative to the body may indicate that the required changes in flight muscle function are small across these changes in flight mode, potentially simplifying the motor control requirements for takeoff and landing flight. Alternatively, different muscles and activation intensities may be required for these different flight modes because gravity always acts downward on the wings, yet the body and wings are oriented horizontally during takeoff and vertically during landing.

The relatively small degree of change in kinematic parameters with respect to the body axis implies that only slight changes are necessary to pitch the body of the bird up or down. Based on the results presented here, we estimated the maximum moment arm necessary to pitch the body of a pigeon upward during the transitions from takeoff to mid-flight and from mid-flight to landing. We assumed angular acceleration of the body during steady flight to be zero and used the body angle and downstroke duration measurements at wingbeat 4 (near the end of takeoff), mid-flight and wingbeat –3 (near the beginning of landing) to estimate maximum angular accelerations. The moment of inertia for pitch of a pigeon was estimated to be $0.00144\,kg\,m^2$ by adjusting measured values (I. G. Ros and A.A.B., unpublished results) for the mass of the birds in this study. Mean body weight, 4.2 N, was used as a minimum value for aerodynamic force. We found that the maximum moment arm from the aerodynamic force vector to the center of mass necessary to pitch the body upward was 1.4 mm from takeoff to mid-flight and 1.7 mm from mid-flight to landing. These remarkably small moment arms suggest that only slight adjustments in kinematics and muscle function are necessary to pitch the body during the transitions between flight phases. Consequently, because the stroke plane, wing plane and tail angles all rotate in concert with the body angle, very subtle changes in kinematics are sufficient to produce major shifts in flight mode. Maintaining longitudinal stability during steady flight would therefore likely require considerable neuromuscular control in the absence of other local or passive stabilizing mechanisms. Further investigation is necessary to determine the mechanisms by which birds maintain longitudinal stability.

To summarize, we found that the pigeon's stroke plane is tilted steeply downward to accelerate the bird during takeoff, but shifts to tilt upward to slow the bird during landing. Importantly, most of the change in local and global SPAs is achieved by body rotation, while the SPA relative to the body remains uniform across the different phases of flight. Wing plane and tail angles also rotate from takeoff to landing, in concert with the body angle. Estimates of the moment arm required to rotate the body suggest that very subtle changes in kinematics can pitch the bird upward during flight. The positioning of the wings, tail and body all appear to contribute to reducing drag or increasing thrust during takeoff, and to increasing drag during landing. The high correlations between body angle and stroke plane, wing plane and tail angles suggest that instead of modifying body posture and stroke orientation, pigeons simply rotate the entire body and thereby direct aerodynamic force more forward during takeoff and more rearward during landing. Analysis of fluid dynamics around pigeons during these maneuvers is needed to confirm these hypotheses and is currently underway. Study of muscle function during flight is also currently underway to investigate whether the simplicity of this mechanism simplifies the muscle control necessary during takeoff and landing.

## LIST OF SYMBOLS AND ABBREVIATIONS

| | |
|---|---|
| $\mathbf{A}_{x,wb}$ | whole-body acceleration in the *x*-direction over the course of one wingbeat |
| $BA_{mds}$ | body angle at mid-downstroke |
| $DSPA_{glob}$ | downstroke plane angle in the global coordinate system |
| DSUS | downstroke–upstroke transition |
| KE | kinetic energy |
| PE | potential energy |
| SPA | stroke plane angle |
| $SPA_{loc}$ | local stroke plane angle |
| $SPA_{relBA}$ | difference between body angle and $SPA_{loc}$ |
| $TA_{mds}$ | tail angle during mid-downstroke |
| USDS | upstroke–downstroke transition |
| $\mathbf{V}_x$ | whole-body velocity in the *x*-direction |
| WBF | wingbeat frequency |
| $\theta$ | downstroke sweep angle |
| $\omega$ | downstroke sweep velocity |

## ACKNOWLEDGEMENTS

We would like to thank the many people at the Concord Field Station who were involved with these experiments, particularly Pedro Ramirez for caring for the pigeons. We also appreciate the helpful comments of two anonymous reviewers. This work was supported in part by NSF grant: IOS-0744056.

## REFERENCES

**Askew, G. N., Marsh, R. L. and Ellington, C. P.** (2001). The mechanical power output of the flight muscles of blue-breasted quail (*Coturnix chinensis*) during take-off. *J. Exp. Biol.* **204**, 3601-3619.

**Berg, A. M. and Biewener, A. A.** (2008). Kinematics and power requirements of ascending and descending flight in the pigeon (*Columba livia*). *J. Exp. Biol.* **211**, 1120-1130.

**Biewener, A. A., Corning, W. R. and Tobalske, B. W.** (1998). *In vivo* pectoralis muscle force-length behavior during level flight in pigeons (*Columba livia*). *J. Exp. Biol.* **201**, 3293-3307.

**Bonser, R. H. C. and Rayner, J. M. V.** (1996). Measuring leg thrust forces in the common starling. *J. Exp. Biol.* **199**, 435-439.

**Brown, R. H. J.** (1948). The flight of birds: the flapping cycle of the pigeon. *J. Exp. Biol.* **25**, 322-333.

**Dial, K. P.** (1992). Activity patterns of the wing muscles of the pigeon (*Columba livia*) during different modes of flight. *J. Exp. Zool.* **262**, 357-373.

**Dial, K. P., Jackson, B. E. and Segre, P.** (2008). A fundamental avian wing-stroke provides a new perspective on the evolution of flight. *Nature* **451**, 985-989.

**Earls, K. D.** (2000). Kinematics and mechanics of ground take-off in the starling *Sturnis vulgaris* and the quail *Coturnix coturnix*. *J. Exp. Biol.* **203**, 725-739.

**Green, P. R. and Cheng, P.** (1998). Variation in kinematics and dynamics of the landing flights of pigeons on a novel perch. *J. Exp. Biol.* **201**, 3309-3316.

**Hatze, H.** (1988). High-precision three-dimensional photogrammetric calibration and object space reconstruction using a modified DLT approach. *J. Biomech.* **21**, 533-538.

**Hedrick, T. L.** (2008). Software techniques for two- and three-dimensional kinematic measurements of biological and biomimetic systems. *Bioinspir. Biomim.* **3**, 1-6.

**Hedrick, T. L., Usherwood, J. R. and Biewener, A. A.** (2004). Wing inertia and whole-body acceleration: an analysis of instantaneous aerodynamic force production in cockatiels (*Nymphicus hollandicus*) flying across a range of speeds. *J. Exp. Biol.* **207**, 1689-1702.

**Rice, W. R.** (1989). Analyzing tables of statistical tests. *Evolution* **43**, 223-225.

**Rosen, M., Spedding, G. R. and Hedenstrom, A.** (2004). The relationship between wingbeat kinematics and vortex wake of a thrush nightengale. *J. Exp. Biol.* **207**, 4255-4268.

**Simpson, S. F.** (1983). The flight mechanism of the pigeon *Columbia livia* during take-off. *J. Zool.* **200**, 435-443.

**Tobalske, B. W. and Biewener, A. A.** (2008). Contractile properties of the pigeon supracoracoideus during different modes of flight. *J. Exp. Biol.* **211**, 170-179.

**Tobalske, B. W. and Dial, K. P.** (1996). Flight kinematics of black-billed magpies and pigeons over a wide range of speeds. *J. Exp. Biol.* **199**, 263-280.

**Tobalske, B. W. and Dial, K. P.** (2000). Effects of body size on take-off flight performance in the Phasianidae (Aves). *J. Exp. Biol.* **203**, 3319.

**Tobalske, B. W., Hedrick, T. L. and Biewener, A. A.** (2003). Wing kinematics of avian flight across speeds. *J. Avian Biol.* **34**, 177-184.

**Tobalske, B. W., Altshuler, D. L. and Powers, D. R.** (2004). Take-off mechanics in hummingbirds (Trochilidae). *J. Exp. Biol.* **207**, 1345-1352.

**Usherwood, J. R., Hedrick, T. L., McGowan, C. P. and Biewener, A. A.** (2005). Dynamic pressure maps for wings and tails of pigeons in slow, flapping flight, and their energetic implications. *J. Exp. Biol.* **208**, 355-369.